Electronic Supplementary Material (ESI) for Nanoscale.
This journal is © The Royal Society of Chemistry 2018

Support Information

Evolution of Surface Catalytic Sites on Thermochemically-Tuned Gold-Palladium Nanoalloys

Haval Kareem,[a] Shiyao Shan,[a] Fang Lin,[a] Jing Li,[a] Zhipeng Wu,[a] Binay Prasai,[b] Casey P. O'Brien,[c] Ivan C. Lee,[c*] Dat Tran,[c] Lefu Yang,[d] Derrick Mott,[e] Jin Luo,[a] Valeri Petkov,[b*] and Chuan-Jian Zhong [a,*]

[a)] Department of Chemistry, State University of New York at Binghamton, Binghamton, NY 13902, USA
[b)] Department of Physics, Central Michigan University, Mt. Pleasant, Michigan 48859, USA
[c)] U.S. Army Research Laboratory, Sensors and Electron Devices Directorate, Adelphi, MD 20783, USA
[d)] College of Chemistry and Chemical Engineering, Xiamen University, Xiamen 361005, China
[e)] School of Materials Science, Japan Advanced Institute of Science and Technology, Nomi, Ishikawa 923-1292, Japan

Additional TEM, characterization, and catalytic activity data:

Atomic PDF G(r) attained through HE-XRD which are sensitive to positioning and number of surface atoms in nanoparticle. PDF peaks at distances represent pair of atoms immediate and all farther neighbors within the NPs and the area of pdf peaks are proportional to the number of atomic pairs. Fundamentally, $G(r)=4\pi r(\rho(r)-\rho_o)$, where $\rho(r)$ and ρ_o are the local and average atomic number density, respectively. Note, as derived, atomic PDFs G(r) are experimental quantities that oscillate around zero and show positive peaks at real space distances, r, where the local atomic density $\rho(r)$ exceeds the average one ρ_o.

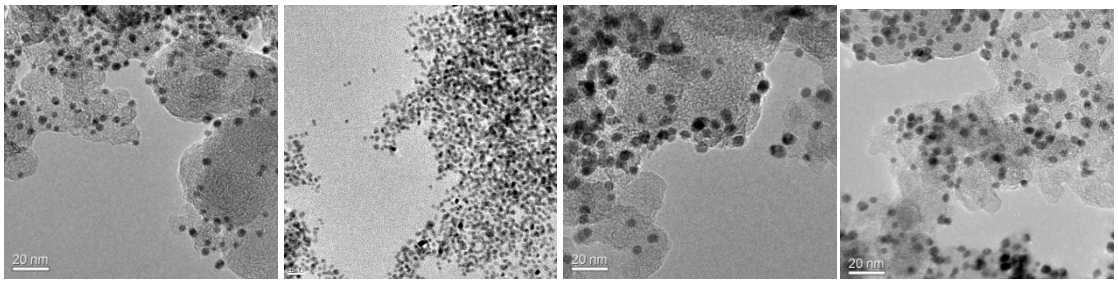

(A) (B) (C) (D)

Fig. S1. TEM images for (A) Au_9Pd_{91}/C (6.5±0.6 nm), $Au_{21}Pd_{79}$ (3.7±0.8 nm), (C) $Au_{45}Pd_{55}$/C (5.5±0.8 nm), and (C) $Au_{69}Pd_{31}$/C (5.3±0.9 nm).

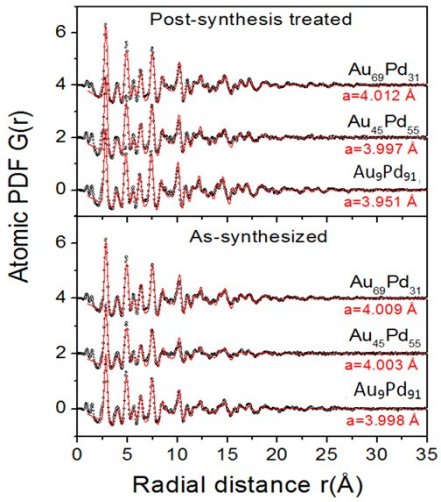

Fig. S2. Experimental (symbols in black) and model (line in red) total atomic PDFs for as-synthesized and post-synthesis thermochemically (under N_2+H_2) treated AuPd /C with three different compositions

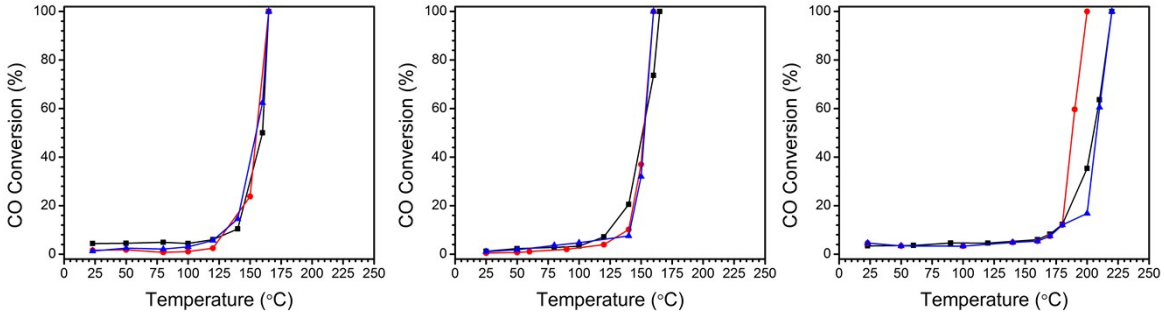

(A) (B) (C)

Fig. S3. CO oxidation activities for carbon-supported Au_9Pd_{91} (A) , $Au_{45}Pd_{55}$ (B), and $Au_{69}Pd_{31}$ (C) catalysts treated under three different conditions: (1) freshly-prepared catalysts (black), 2) catalysts treated under O_2 at 260 °C for 0.5 hr (red), and (3) catalysts treated under H_2 at 400 °C for 0.5 hr (blue). (The standard deviation of the data is ± 1.8)

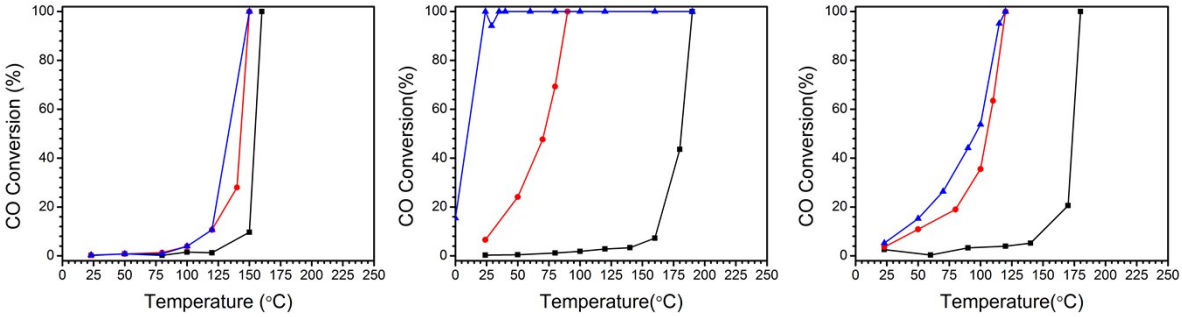

(A) (B) (C)

Fig. S4. CO oxidation activities for TiO_2-supported Au_9Pd_{91} (A) , $Au_{45}Pd_{55}$ (B), and $Au_{69}Pd_{31}$ (C) catalysts treated under three different conditions: (1) freshly-prepared catalysts (black), 2) catalysts treated under O_2 at 260 °C for 0.5 hr (red), and (3) catalysts treated under H_2 at 400 °C for 0.5 hr (blue). (The standard deviation of the data is ± 1.8).

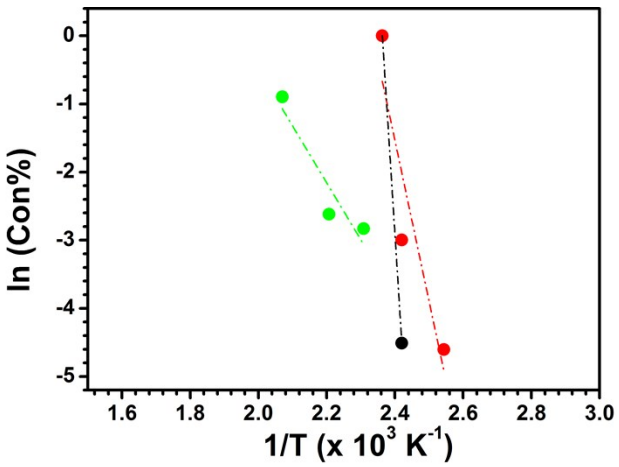

Fig. S5. Arrhenius plot for CO oxidation over Au_9Pd_{91}/C catalysts:fresh state (black), after O_2 treatment (red), and after H_2 treatment (green).

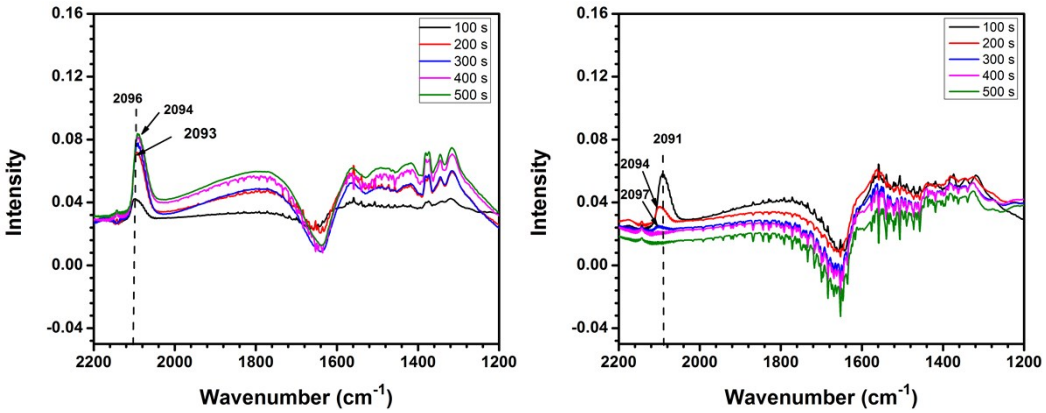

(A) (B)

Fig. S6. In-situ DRIFTs spectra for CO adsorption at room temperature over commercial Au/TiO_2 catalyst as a function of time: under CO exposure (A), and followed by N_2 purge (B).

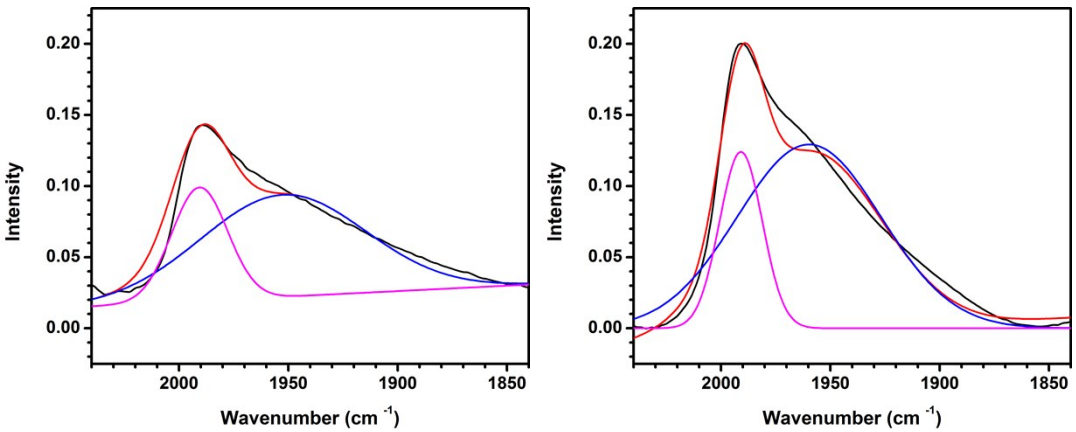

(A) (B)

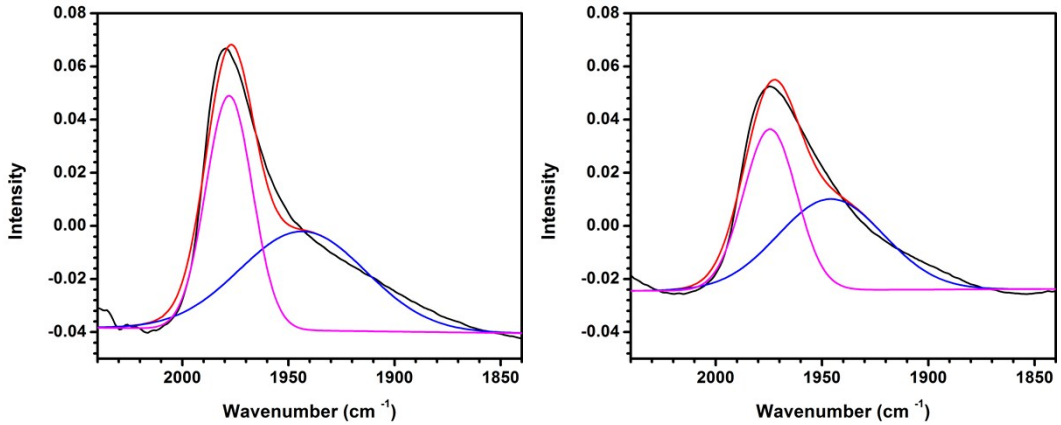

Fig. S7. A representative set spectral devonvolution based on two peaks for the spectra collected under CO + O_2 reaction condition at different temperatures over $Au_{45}Pd_{55}/TiO_2$ catalyst after thermal treatment in O_2 at 260 °C for 30 min (top pannel) and thermal treatment in H_2 at 400 °C for 30 min (bottom pannel): at room temperature (A and C), and at 100 °C (B and D).

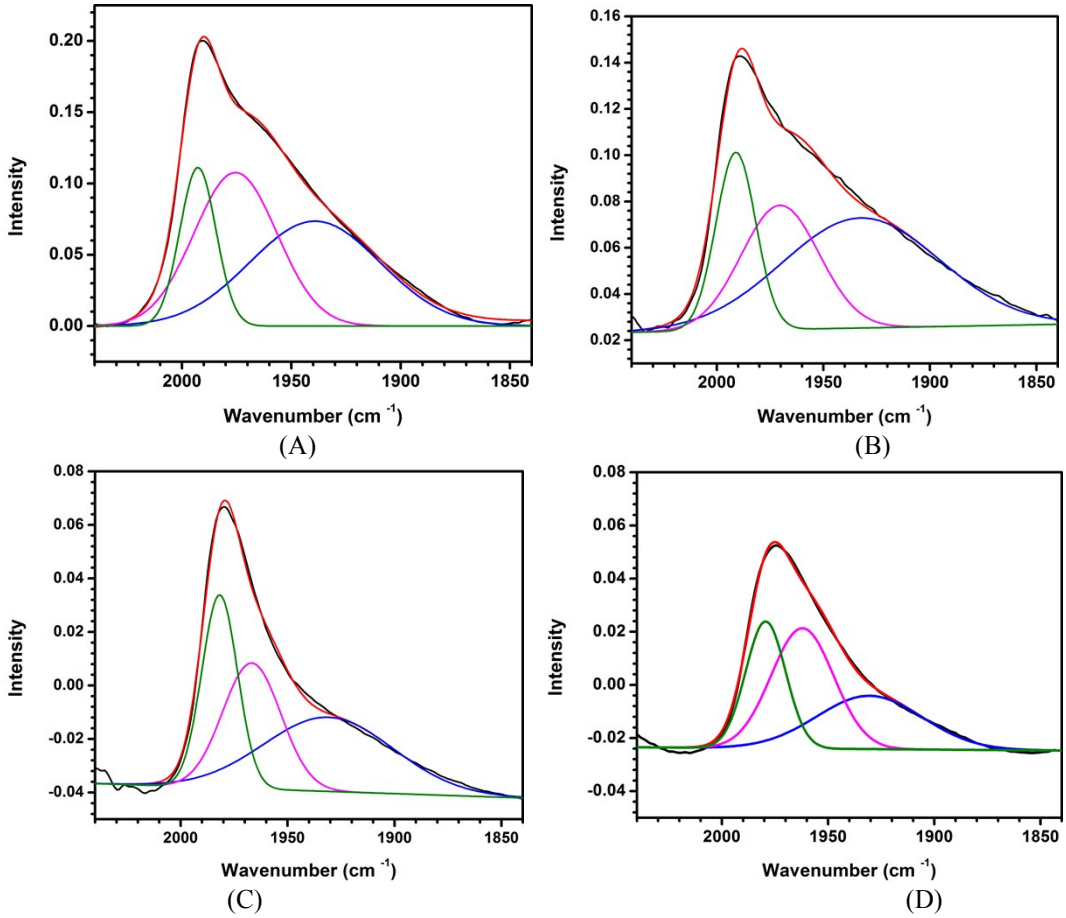

Fig. S8. A representative set of spectral devonvolution based on three peaks for the spectra collected under CO + O_2 reaction condition at different temperatures over $Au_{45}Pd_{55}/TiO_2$ catalyst after thermal treatment in O_2 at 260 °C for 30 min (top pannel) and thermal treatment in H_2 at 400 °C for 30 min (bottom pannel): at room temperature (A and C), and at 100 °C (B and D).

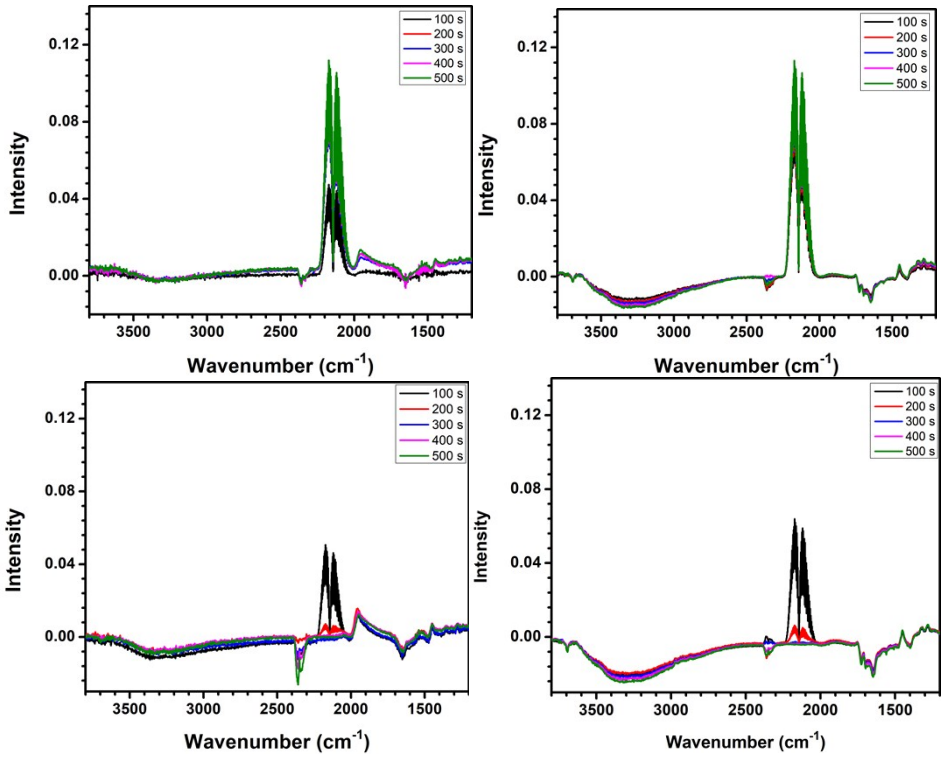

(A) (B)

Fig. S9 In-situ real-time DRIFTs spectral evolution of CO adsorption at room temperature over AuPd catalysts of different compositions: (A) Au_9Pd_{91}/TiO_2, and (B) $Au_{69}Pd_{31}/TiO_2$. Top panel: under CO exposure; Bottom panel: under N_2 purge following the CO exposure. Both spectra were not corrected against the spectrum of TiO_2 .

Table S1. Activation energy vs. Au% (n) for CO oxidation over AuPd /C (A) and AuPd /TiO_2 under O_2 treatment at 260 °C for 30 min; and under H_2 treatment at 400 °C for 30 min

Catalyst	E_a(kJ/mol) (under O_2 treatment)	E_a(kJ/mol) (under H_2 treatment)
Au_9Pd_{91} /C	207	204
$Au_{45}Pd_{55}$ /C	195	94
$Au_{69}Pd_{31}$ /C	50	60
Au_9Pd_{91} /TiO_2	120	120
$Au_{45}Pd_{55}$ /TiO_2	34	6
$Au_{69}Pd_{31}$ /TiO_2	58	32

Table S2. DFT-calculated adsorption energy (eV) for molecularly adsorbed CO on a (111)-slab model of Au_nPd_{48-n} surface layer (n = 0, 4, 22, 33, and 48). Pd (green), Au (light blue), carbon (gray), and oxygen (red)

	Pd_{48}	**Au_4Pd_{44}**	**$Au_{22}Pd_{26}$**	**$Au_{33}Pd_{15}$**	**Au_{48}**
Structure model for CO adsorption on a (111)-surface	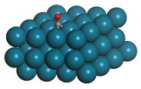	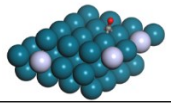	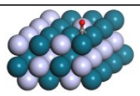		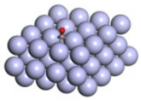
Adsorption energy (eV)	1.85	1.86	1.96 (1.96 on 3-fold Pd site, 1.57 on bridge pd site, and 1.34 on atop Pd site)	1.49	0.28